IEEE Access
Multidisciplinary | Rapid Review | Open Access Journal

Received April 28, 2020, accepted May 5, 2020, date of publication May 8, 2020, date of current version May 21, 2020.

Digital Object Identifier 10.1109/ACCESS.2020.2993322

Total Variation Filter via Multiquadric Radial Basis Function Approximation Scheme for Additive Noise Removal

MUSHTAQ AHMAD KHAN[1], AHMED B. ALTAMIMI[2], ZAWAR HUSSAIN KHAN[3], KHURRAM SHEHZAD KHATTAK[3], MURTAZA ALI[1], ASMAT ULLAH[3], SHERAZ KHAN[1], MUHAMMAD SOHAIL KHAN[1], AND MUHAMMAD FAISAL ABRAR[1]

[1]University of Engineering and Technology Mardan, Khyber Pakhtunkhwa 23200, Pakistan
[2]University of Hail, Hail 81451, Saudi Arabia
[3]University of Engineering and Technology Peshawar, Khyber Pakhtunkhwa 25000, Pakistan

Corresponding author: Mushtaq Ahmad Khan (mushtaq@uetmardan.edu.pk)

ABSTRACT The Digital Total Variation (DTV) scheme is a digitized energy regularization scheme used for image denoising. This technique takes advantage of being applied to arbitrarily located data points and also has the edge detective property. This article aims to introduce a novel meshless scheme using DTV filtering and Radial Basis Functions (RBFs) to solve the associated equation with the DTV model numerically which results in the image denoising to remove additive noise from image information. This meshless algorithm based on local collocation and Multiquadric Radial Basis Function. These appearances allow this algorithm not only to remove the additive noise from images but also to resolve the discontinuities sharply. It is also noticed that the proposed meshless scheme is simple, fast, computationally effective, requires simply post-processing, and can be easily implemented mathematically. Experimental results confirm that the peak signal-to-noise ratio, the structural similarity, signal-to-noise ratio, the visual effect, and the computational performance of this new meshless scheme are improved compared with state-of-the-art denoising schemes. Furthermore, the proposed scheme can be applied to colour images as well.

INDEX TERMS Image denoising, digital total variation (DTV) filter, multiquadric radial basis function (MQ-RBF), restoration equation, traditional scheme, meshless scheme.

I. INTRODUCTION

Image denoising is one of the most powerful aspects of image processing and computer vision. This paper concentrates on the additive noise removal. Image denoising is to remove noise from a noisy image, to restore the true image. Nevertheless, as noise, edge, and texture are high frequency elements, it is complicated to identify them in the process of denoising and the denoised images could necessarily lose some details. In general, recovering important information from noisy images in the process of noise removal to obtain high quality images is an essential problem nowadays [1].

The additive noise removal problem is modeled as

$$z_0 = z + \eta, \tag{1}$$

where z: $\Omega \subset R \longrightarrow R^2$ represents the given true image, z_0 is the noisy image with additive noise η. In literature, various nonlinear approaches have been utilized to tackle this problem, such as wavelet approaches [2]–[4], adaptive smoothing [5], [6], stochastic approaches [7], [8], anisotropic diffusion [9], [10]. Recently variational approaches have also been utilized to solve such problem, for instance [11]–[13]. In conventional variational approaches, the Euler-Lagrange PDE is obtained from the minimization functional of equation (1) is used for smooth solution of image denoising. But the Euler-Lagrange PDE is always a nonlinear and non-differential PDE equation. Therefore the classical numerical schemes unsuccessful to solve the PDE equation for the smooth solution, which produces staircase effects, textures, and degrading the fine details during the image denoising process. Some numerical scheme have been utilized by the researchers to minimize the above mentioned issues such as Augmented Lagrangian Method (ALM) [14], [15],

The associate editor coordinating the review of this manuscript and approving it for publication was Gerardo Di Martino.

This work is licensed under a Creative Commons Attribution 4.0 License. For more information, see https://creativecommons.org/licenses/by/4.0/

Dual Method (DM) [16], Variable Splitting Based Method (VSBM) [17], and Alternating Direction Method of Multipliers (ADMM) [18]. But Still there is a space for improvement.

Various filter-based approaches have been introduced based on these IN detectors, for instance, adaptive center-weighted median filter [19], progressive switching median filter [20], adaptive weighted median filter (AWMF) [21], noise adaptive fuzzy switching median filter (NAFSMF) [22], modified decision- based unsymmetrical trimmed median filter (MDBUTMF) [23], and morphological mean filter (MMF) [24]. These filter-based approaches are smoothly useful in image denoising and reducing the staircase effect, textures and homogeneity in lightly contaminated noisy images. Nevertheless, these schemes are ineffective for reducing noise in highly corrupted images (i.e., noise frequency greater than or equal to 50 percent) because of the inaccuracy of order statistics.

Chan *et al.* [25] introduced a self-contained 'digital' (Digital total variation (DTV))filtering theory for image denoising which is independent of the experience of PDEs and numerical solution. DTV filtering is acknowledged as a discrete variational approach that works on the general discrete domain of given data. This approach is more responsive to regular and irregular shaped domains, and the scattered data points can easily be managed. Another benefit of this scheme is to determine the discontinuities sharply without earlier information concerning edge locations due to its built-in edge detective property [25], [26], [28]. DTV filtering procedure is a general method in comparison with other pseudospectral post-processing schemes, so it does not require the location of data on the structured grid [29]–[31]. The DTV filtering approach has been used for the steady-state solutions of conservation of law computed by second-order Lax-Wendro methods [28], [30], [32]. The associated restoration equation to DTV functional of the model (1) is always nonlinear. Recently, some numerical schemes have been produced for the numerical solutions of DTV based nonlinear equation for smooth solutions i.e. to remove the noise and restore the accuracy of the given image information, for instance, see [25], [27]–[29], [31]. But when the noise variance becomes high, the fine details of the image can not be recovered properly, which is the principal disadvantage of the solution of DTV filtering by classical numerical techniques. To the best of our knowledge, few numerical schemes have been utilized to solve the DTV based nonlinear equation and to tickle this issue. In this study, we will introduce a meshless algorithm for the numerical solution of DTV based nonlinear equation to settle as the issues associated with image denoising.

Radial basis function (RBF) methods have become successful methods in recent years in approximation theory as well as in the numerical solution of PDEs. The most broadly applied RBF scheme for the latter class of problems is the RBF collocation method due to Kansa [33]–[35], known as the Kansa method. The popularity of the Kansa approach is due to its meshless applications which means that only a set of points is required in the discretization of the continuous problem. This contribution to the implementation of the method particularly easy, especially for problems in the complex shape domain, and in two and more dimensions. The solution of the nonlinear problem hence produces not only the coefficients in the RBF approximation but also a suitable value of the shape parameter [36]. Kansa method has also shown excellent efficiency compared to FDM [35], [37], pseudo-spectral method [38], and FEM [39]. Since, Kansa method is a domain type strategy, which has numerous features like the finite element approach for the approximated solution of the nonlinear equation. For further information of RBF collocation schemes, see [36], [40]–[44]. In this research study, we will use the BRF meshless collocation scheme (Kansa scheme) for the solution nonlinear equation arising in the DTV filtering based model [25]. Since, Kansa method is a domain type strategy, which has numerous features like the finite element approach for the approximation of the solution of the nonlinear equation. This proposed scheme will not only be helpful in image denoising and edge preservation but also be helpful in the minimization of staircase effect, preservation of textures, and fine details during the restoration process. The main purposes of the recommended meshless scheme in image restoration are; the RBF interpolation process used in the proposed scheme will preserve the edges and fine details in images while the smoothness property and the lack of dependence on a mesh or integration procedure will produce the best restoration performance regarding minimization of staircase effect and texture preservation.

The paper outlines are organized as follows. The detailed mathematical discussion of DTV filtering and RBFs approximation is given in section. The discussion of Chan *et al.* [25] model for image denoising having additive noise is also mentioned in section 2. The mesh-based scheme and proposed meshless scheme for the solution of the model [25] are discussed in section 22. Section 4 describes some numerical results to validate the performance of the proposed scheme. A comparison with existing state-of-art numerical schemes is described in section 5. Section 5 shows the detailed tabulated discussion of the sensitivity of parameters used in the proposed technique. Finally, the paper is concluded in the last section.

II. MATHEMATICAL BACKGROUND

A. DIGITAL TOTAL VARIATION FILTERING

To define DTV filtering [25], let select a general graph [Ω,D], containing a finite set of Ω having different nodes (vertices) and a dictionary D of edges. In the graph, the size of D represents the total number of nodes (vertices). It is also assumed that the graph is associated and has no self-loops (no immediate edge from a vertex to itself). All the general vertices on the graph are named $\beta_1, \beta_2, \ldots$. The notation $\beta_1 \sim \beta_2$. indicates that β_1 and β_2 are neighbors. All the neighbors of β_1 are represented by $N_{\beta_1} = \{\beta \in \Omega \mid \beta_1 \sim \beta_1\}$ for $\beta_1 \sim \beta_1 = \beta_2 \sim \beta_1$. Let z such that $z : \Omega \longrightarrow R$

denotes the digital image, for any vertex β_1, $z_{\beta 1}$ signifies the z at vertex β_1. At any vertex β_1, the regularized local variation or strength function $\|\nabla_p z_{\beta_1}\|$ is defined as

$$\left\|\nabla_p z_{\beta_2}\right\| = \left[\sum_{\beta_2 \in N_{\beta_1}} \left(z_{\beta_2} - z_{\beta_1}\right)^2\right]^{\frac{1}{2}}. \tag{2}$$

To avoid the regularized local variation from zero denominator, a small regularization parameter α is selected, thus the equation (2) can be re-written as

$$\left\|\nabla_p z_{\beta_2}\right\| = \left[\sum_{\beta_2 \in N_{\beta_1}} \alpha^2 + \left(z_{\beta_2} - z_{\beta_1}\right)^2\right]^{\frac{1}{2}}.$$

As explained in [25], the edge derivative of z is given as under.

$$\left.\frac{\partial z}{\partial e}\right|_{\beta_1} := z_{\beta_2} - z_{\beta_1},$$

where e denotes the edge of z along e and is represented by $\beta_2 \sim \beta_1$. Also

$$\left.\frac{\partial z}{\partial e}\right|_{\beta_1} = \left.\frac{\partial z}{\partial e}\right|_{\beta_2} \quad \text{and} \quad \left\|\nabla_p z_{\beta_1}\right\| = \sqrt{\sum_{e \vdash \beta_1} \left[\left.\frac{\partial z}{\partial e}\right|_{\beta_1}\right]^2},$$

where $e \vdash \beta_1$ shows that β_1 is one node of e. For more information about DTV filtering, see [25], [29], [31].

The first DTV filtering based minimization model for image denoising having additive noise was presented by Chan *et al.* [25]. So, equation (1) by [25] can be re-written as

$$z_0 = z + \eta \quad or \quad z^0_{\beta_1} = z_{\beta_1} + \eta_{\beta_1}, \tag{3}$$

for all $\beta_1 \in \Omega$, where z is restored image data, z_0 is noisy image data with additive noise data η. The minimization approach for equation (3) by [12], [25] is defined as;

$$\min_z E(z) = \sum_{\beta_1 \in \Omega} \left\|\nabla_p z_{\beta_1}\right\| + \frac{\lambda}{2}\left\|z_{\beta_1} - z^0_{\beta_1}\right\|^2_{\Omega}. \tag{4}$$

In the foregoing equation (4), the first term is the regularization term, while the second term is the data fidelity term, where γ and α are called the fitting and regularization parameters, respectively.

B. RADIAL BASIS FUNCTION APPROXIMATION

The RBF collocation scheme is defined as, a RBF function $\phi(x)$ with respect to the origin, $\phi(x) = \phi(r) \in \Re$ for the known data set $\{x_j\}$ and its distance from a given point (pixel) such that with $\phi(x - x_j) = \phi(r_j) \in \Re$ is satisfied. The function $\phi(x) = \phi(\| x \|_2)$ is known as radial function. The different basis functions that are used in RBF collocation method are Multiquadric (MQ), Inverse Multiquadric (IMQ), Gaussian (GA), Polyharmonic spline, and Thin plate splines (TPS). For more information regarding these basis functions, see [45], [46].

The RBF collocation scheme is used on function $f(x)$, $x \in \Omega \in \Re^n$ including bounded domain Ω to interpolate it smoothly. So, for the given selected interpolating values data centers points, the function is approximated as under.

$$f(x) = \sum_{j=1}^{N} \gamma_j \phi\left(\left\|x - x_j\right\|_2\right), \quad x \in \Omega, \tag{5}$$

where γ_j are defined weights. To calculate γ_j, the RBF scheme is defined as

$$y_i = f(x_i) = \sum_{j=1}^{N} \gamma_j \phi\left(\left\|x_i - x_j\right\|_2\right), \quad i, j = 1, 2, \ldots, N. \tag{6}$$

The above equation (6) gives a linear system of equations of order $N \times N$ which is written as under.

$$C = \gamma b,$$

where $\gamma = (\gamma_1, \gamma_2, \ldots, \gamma_N)^T$ is known as $N \times 1$ undefined vector and to be defined, while $b = (y_1, y_2, \ldots, y_N)^T$ is $N \times 1$ known vector, and $C = [\phi_{i,j}] = [\phi(\|x - x_j\|_2)]_{1 \le i,j \le N}$ with $\phi_{ij} = \phi_{ji}$ is called $N \times N$ interpolation matrix.

The polynomial term is added to the RBF approximation to ensure invertibility of the interpolated matrix C, in such case equation (5) can be defined as under.

$$f(x) = \sum_{j=1}^{N} \gamma_j \phi\left(\left\|x - x_j\right\|_2\right) + \sum_{i=1}^{M} \gamma_{N+1} l_i(x), \tag{7}$$

with constraints

$$\sum_{i=1}^{M} \gamma_j l_i(x_j) = 0, \quad i = 1, 2, \ldots, M, \tag{8}$$

with $l_i \in \Pi_{m-1}$ for $i = 1, 2, \ldots, M$, in which Π_m represents the polynomial space in which the polynomial is m in N variables are the total degree polynomials [45], which is given as

$$\begin{bmatrix} N + m - 1 \\ m - 1 \end{bmatrix}.$$

The resultant solution of equations (7) and (8) through interpolation gives matrix system of $(M+N) \times (M+N)$ equations which is given as under.

$$\begin{bmatrix} C & l \\ l^t & O \end{bmatrix} = [\gamma] \begin{bmatrix} b \\ 0 \end{bmatrix},$$

where $C = [\phi_{i,j}] = [\phi(\|xi - x_j\|_2)]_{1 \le i,j \le N}$ shows the elements of the matrix C, $l_{i,j} = l_i[x_j]_{1 \le i \le N, 1 \le j \le M}$ are the elements of the matrix l, and O is $(M \times N)$ matrix.

The RBFs having shape parameter c and selection of shape parameter, also the RBFs having positive definiteness (PD) and conditionality positive definiteness (CPD) are explained in [45], [47]. The selection of shape parameter c in RBFs, positive definiteness in RBFs, and Conditionality positive definiteness CPD are described in [45], [47].

III. NUMERICAL SCHEMES

IIn this section, numerical schemes are reviewed for the numerical solution of the system of nonlinear equations connected with the DTV minimization functional (4).

A. MESH-BASED SCHEME M1

The primary DTV filter-based model was introduced by Chan *et al.* [25] for image restoration containing additive noise and produced some good recovery results on a 1-D graph and 2-D images (grayscale), and 3-D (color) images. The minimization functional for [25] from equation (4) is mathematically written as,

$$\min_{z} E(z) = \sum_{\beta_1 \in \Omega} \left\| \nabla_p z_{\beta_1} \right\|_{\alpha} + \frac{\lambda}{2} \left\| z_{\beta_1} - z^0_{\beta_1} \right\|^2_{\Omega}, \tag{9}$$

where the first term is called regularization term, the second term is called data fidelity term and γ is the fitting parameter and α is regularized parameter. The fidelity parameter γ is used to set a balance between the denoised and smoothness of the denoised images which is often based on the level of noise added to the given image and the regularization parameter α is used to avoid a zero so its value is usually taken $\alpha = 10^{-4}$. The resultant nonlinear restoration equation from (9) by [25] is given as

$$0 = \sum_{\beta_2 \sim \beta_1} \left(z_{\beta_1} - z_{\beta_2} \right) \omega_{\beta_1 \beta_2}(z) + \lambda \left(z_{\beta_1} - z^0_{\beta_1} \right), \tag{10}$$

where

$$\omega_{\beta_1 \beta_2} = \frac{1}{\| \nabla_p z_{\beta_1} \|_{\alpha}} + \frac{1}{\| \nabla_p z_{\beta_2} \|_{\alpha}}, \tag{11}$$

and

$$\| \nabla_p z_{\beta_2} \| = \left[\alpha^2 + \| \nabla_p z_{\beta_2} \| \right]^{\frac{1}{2}}. \tag{12}$$

for a small fixed value of α i.e., $\alpha = 10^{-4}$. The above equation (10) can be fixed and re-defined as

$$0 = \sum_{\beta_2 \sim \beta_1} \left(z_{\beta_1} - z_{\beta_2} \right) \left[\frac{1}{\| \nabla_p z_{\beta_1} \|_{\alpha}} + \frac{1}{\| \nabla_p z_{\beta_2} \|_{\alpha}} \right] + \lambda \left(z_{\beta_1} - z^0_{\beta_1} \right). \tag{13}$$

For further details, see in [25], [27], [28].

B. PROPOSED MESHLESS SCHEME M2

In this new subsection, we introduce the meshless scheme by applying the BRF collocation scheme for the numerical solution of DTV filter-based restoration equation (12) and to get resultant image z from the given noisy image z_0 selected in model (9). Consider $\{\beta_j\}_{j=1}^{Nc}$ be Nc centers in the closed domain $\Omega \subseteq \Re^2$. For any RBF in 2D (2 Dimensional), the following equation will be satisfied, $\phi(r) = \|r\|_2$ in $\Re^2$ i.e $r = (x, y)$.

For given pixel data center points $\{\beta_j\}_{j=1}^{Nc}$, the equation for RBF approximation with unaugmented polynomial term is given as below.

$$H(x) = \sum_{j=1}^{Nc} \theta_j \phi(\|x - \beta_j\|_2), \tag{14}$$

with undefined coefficients of θ_j and are defined the given interpolation condition.

$$H(x_j) = z^0.$$

The RBF interpolation at Nc centers data is written as

$$D\theta = z^0, \tag{15}$$

which results in $Nc \times Nc$ linear system of equations. This system is used to find the coefficients of $Nc \times 1$ vector $\theta = (\theta_1, \theta_2, \ldots \theta_{Nc})^T$ for given known vector data $z_0 = (z^0_1, z^0_2, \ldots z^0_{Nc})^T$, where

$$D = [\phi_{i,j}] = [\phi(\|x_i - x_j\|_2)]_{1 \le i,j \le Nc},$$

is called $Nc \times Nc$ matrix and is an invertible matrix [30], [47] due its positive definite application [43], [45]. Thus

$$\theta = D^{-1} z^0, \tag{16}$$

with θ represents a $Nc \times 1$ order matrix. Again using the same above-mentioned operation on equation (14), the RBF interpolation at N evaluation points $\{x_i\}_{i=1}^{N}$ results in $Nc \times N$ matrix E which is defined as follow.

$$E = [\phi_{i,j}] = [\phi(\|x - x_j\|_2)]_{1 \le i \le N, \quad 1 \le j \le Nc}.$$

The resultant equation to obtain z at N data points using interpolation is given as,

$$z = E\theta. \tag{17}$$

The combination of equations (15) and (16) results in the given equation.

$$z = ED^{-1} z^0,$$

or

$$z = Lz^0 \quad where\ L = ED^{-1}, \tag{18}$$

which results in approximate solution of at any point inside the closed domain Ω. Since equation (10) forms the minimization functional (4) of model [25] using DTV method and is given as

$$0 = \sum_{\beta_2 \sim \beta_1} \left(z_{\beta_1} - z_{\beta_2} \right) \omega_{\beta_1 \beta_2}(z) + \lambda \left(z_{\beta_1} - z^0_{\beta_1} \right), \tag{19}$$

where

$$\omega_{\beta_1 \beta_2} = \frac{1}{\| \nabla_p z_{\beta_1} \|_{\alpha}} + \frac{1}{\| \nabla_p z_{\beta_2} \|_{\alpha}}.$$

The steady state time marching equation from equation (18) is denoted by the equation below.

$$\frac{dz_{\beta_1}}{dt} = \sum_{\beta_2 \sim \beta_1} \left(z_{\beta_1} - z_{\beta_2} \right) \omega_{\beta_1 \beta_2}(z) + \lambda \left(z_{\beta_1} - z^0_{\beta_1} \right). \tag{20}$$

The Collocation method (Kansa scheme) is then used to solve the obtained restoration equation by the combination of the equations (17) and (19). Here Gauss-Jacobi iterative is used in Kansa scheme to solve resultant system of non linear equation which is given as follow.

$$z_{\beta_1}^{(n+1)} = z_{\beta_1}^{(n)} + dt\Bigg[\sum_{\beta_2 \sim \beta_1}\left(z_{\beta_2}^{(n)} - z_{\beta_1}^{(n)}\right)\omega_{\beta_1\beta_2}(z^{(n)}) + \lambda\left(z_{\beta_1}^{(n)} - z_{\beta_1}^{(0)}\right)\Bigg], \quad (21)$$

where $z_{\beta_1}^{(0)} = z_{\beta_1}^{0}$, $z_{\beta_1} = L_{\beta_1}z^0 = E_{\beta_1}D^{-1}z^0$, and $z_{\beta_2} = L_{\beta_2}z^0 = E_{\beta_2}D^{-1}z^0$. Also

$$E_{\beta_1} = [\phi_{\beta_1 j}] = [\phi(\|\beta_1 - \beta_j\|_2)]_{1\le j\le Nc},$$

and

$$E_{\beta_2} = [\phi_{\beta_2 j}] = [\phi(\|\beta_2 - \beta_j\|_2)]_{1\le j\le Nc}.$$

Here $z_{\beta 1}$ and $z_{\beta 2}$ represent the approximate values at vertices $\beta 1$ and $\beta 2$ respectively. The main application of the RBF scheme (Kansa method) is usually not necessary to satisfy the given restoration equation (21), so we are independent to choose any BRF. In literature, multiquadric (MQ) RBF gives good results in the RBF scheme (Kansa method) [34], [48] provided if a proper value for shape parameter is chosen [34]. The main utilization of the collocation scheme used on equation (21) is that the suggested meshless method displays the unique solution of (21) due to the MQ-RBF interpolation method employed in the collocation scheme which results in the preservation of the edges. Furthermore, the resultant smooth solution of equation (21) is due to the weighted mean determined in equation (15) using the interpolation process which is based on the Euclidian distance between a noisy pixel and other non-noisy pixels obtained from equation (14) in the selected frame. Consequently, the smooth solution of the equation (21) is responsible for image restoration, reducing the staircase effect, and preserving edges, textures, and image details. In our proposed meshless scheme M2 the value of shape parameter c plays an important role in smooth solution in terms of good image restoration result. In our meshless technique, c and λ are important parameters for good restoration results and their values are based on the image size and noise. The locality and adaptivity for smooth results by DTV filtering have already been discussed in [25].

Many research papers have been published by the researchers regarding the selection of the best value of shape parameter c for getting the smooth results used in RBF. Here, we will apply the extended Rippa's [49] algorithm proposed by Marjan [50] for the selection of the best value of MQ shape parameter c used in the proposed meshless scheme M2, which is shown in algorithm2. All entries in the error vector ϵ can be computed in a single statement in MATLAB. In order to determine a good value of the shape parameter as quickly as possible we have used the Matlab function **fminbnd** to find the minimum of the cost function $\|\epsilon\|$ for c The algorithm returns a good value $c \in (c_{min}, c_{max})$ where $c_{min} = \frac{7}{\sqrt{N}}$ and $c_{max} = \frac{15}{\sqrt{N}}$ are chosen initially. In this article, the role of algorithm 2 in our meshless algorithm 1 is to find the optimal value of c to provide the best restoration performance in terms of PSNR value rather than error estimation.

Algorithm 1 Algorithm for Proposed Meshless Scheme M2

Radial Basis Function Approximation:

1. Set the centers $\beta_1, \beta_2, \ldots \beta_{|\Omega|}$.
2. Use MQ-RBF to calculate θ by using (16).
3. Use MQ-RBF to calculate z by using (18).

DTV filtering:

4. Choose the centers $\beta_1 \le \beta_2 \le, \ldots, \le \beta_{|\Omega|}$, let $n = 0$.
5. $n = n + 1$, for the selection of each center location β_1 and all its neighbors β_2, calculate the local variation $\|\nabla_p z_{\beta_2}\|_\alpha$ and weighted function $\omega_{\beta_1\beta_2}(z^{(n)})$ according to equation (12) and (11).
6. Put $\omega_{\beta_1\beta_2}(z^{(n)})$ and $z^{(n)}$ in equation (21) to get $N \times 1$ nonlinear system of equations.
7. For each located center β_1, calculate $z_{\beta_1}^{(n+1)}$ by using equation (21), where we choose $z^{(0)} = z^0$.
8. $\frac{\|g^{(n+1)} - g^{(n)}\|}{\|g^{(n)}\|} \le \epsilon = 10^{-5}$ (stopping condition for iterations), go to step no. (11).
9. Back to step no.(5).
10. End.
11. Outcome result $z = z_{\beta_1}^{(n+1)}$.

Algorithm 2 Algorithm for the Selection of Shape Parameter c in Meshless Scheme M2

:

1. Fix $c \in (c_{min}, c_{max})$
2. For $n = N + 1$, compute the error estimator ϵ_n at the *nth* data point from equation (16) by the relation $\epsilon_n = \frac{\theta_n}{D_n^{-1}}$.
3. Get the cost vector $\epsilon = (\epsilon_1, \epsilon_2, \ldots, \epsilon_n)^T$.
4.End.
5. The optimal value of c is obtained by the minimization of $\|\epsilon\|$.

IV. EXPERIMENTAL RESULTS

In this section, experimental analysis is demonstrated to validate the performance of the proposed meshless collocation scheme M2. To justify the performance of the meshless method M2, we perform several experiments on real and artificial grayscale and color images and compare the results with a classical method M1. The test images for experimental analysis are shown in Fig.1. For 2D case, N_β can be defined in different ways. One way is to consider a point P neighbor of a node β consisting of all P points that are closest to β. In this paper, N_β is defined in the best way. Dividing the region surrounding a point an into P regions of equal angle, N_β is defined such that it consists of points in each region that are closest to β as discussed in [25]. In this research study,

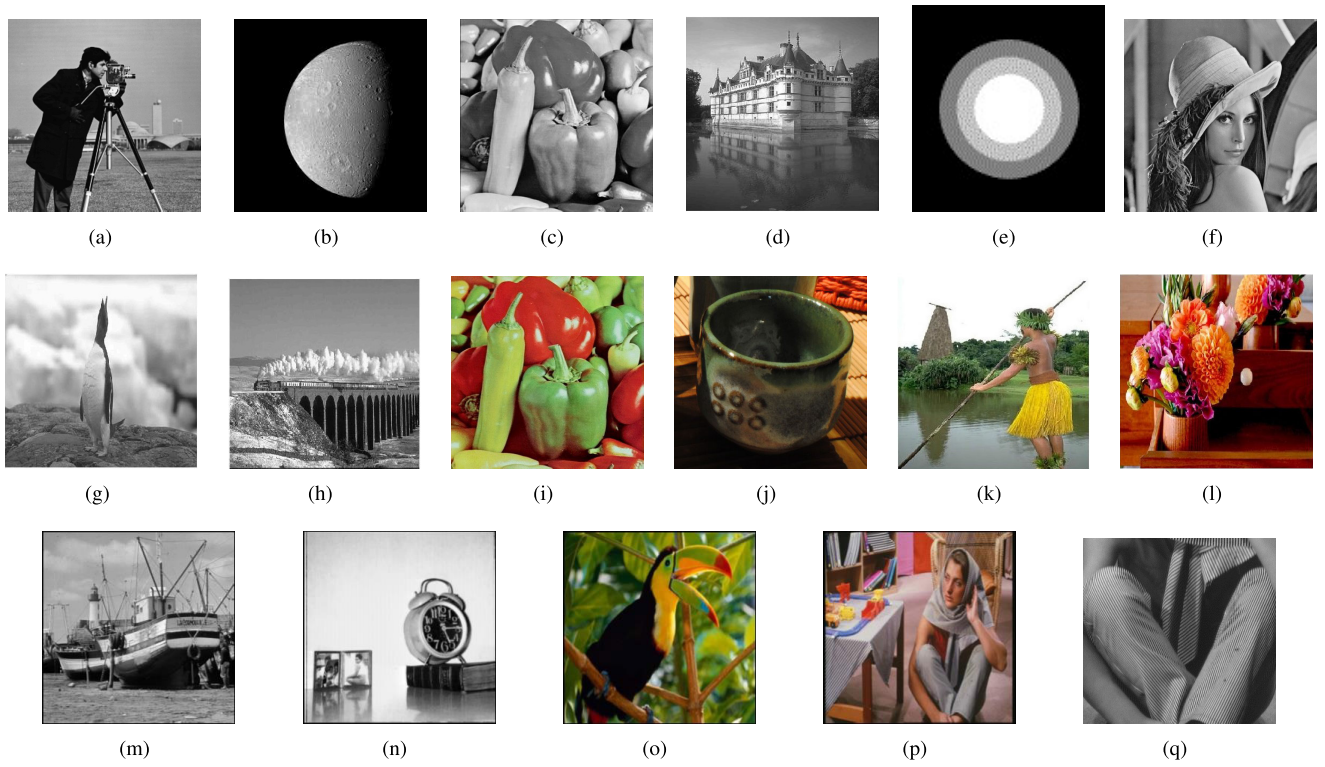

FIGURE 1. Test images; (a) Cameraman; (b) Moon; (c) Peppers; (d) House; (e) Ring; (f) Lena; (g) Bird; (h) Bridge; (f) Colour Peppers; (i) Colour Sanada; (j) Colour Man; (k) Colour Rose; (l) Boat; (m) Clock; (n) Colour Bird; (o) Colour barbara; (p) Barbara.

we select P as the size of the chosen image and Multiquadric Radial Basis Function (MQ-RBF) is utilized as the basis function for meshless scheme M2. The peak-signal-to-noise ratio (PSNR) is used to determine the quality of the denoised image. PSNR of an image can be calculated by the following formula.

$$PSNR = 10 * log_{10}\left[\frac{M \times N\ max\{\hat{u}\}}{\|\hat{u} - u\|}\right]. \tag{22}$$

where $\hat{u}$ is the selected image and u represents the denoised image, while $M \times N$ is the size of the selected image.

The Structure Similarity (SSIM) index is a method for estimating the similarity between two images [51], [52]. It carries the necessary information for image quality evaluation utilizing the principle approach that the pixels have storing interdependency when they are spatially close. The SSIM metric is based on the intensity, contrast, and structure, and is determined as

$$SSIM(u, v) = \frac{(2\mu_u\mu_v + c_1)(\sigma_{uv} + c_2)}{(\mu_u^2 + \mu_v^2 + c_1)(\sigma_u^2 + \sigma_v^2 + c_2)}, \tag{23}$$

where μ_u, μ_v, σ_u, σ_v, σ_{uv} indicate the mean, variance, and covariance on typical 8×8 square windows, which movies pixels by pixels in images $u(i)$ and $v(i)$, respectively. The two variables $c_1 = k_1L$ and $c_2 = k_2L$ are employed to stabilize the division with weak denominator. Here, L is the dynamic range of pixel value (e.g., 255 for 8-bit grayscale image), with $k_1 = 0.01$ and $k_2 = 0.03$ by default. As the SSIM metric is measured on various windows of an image, the mean SSIM (MSSIM) is used in this experiment to evaluate the overall image quality:

$$MSSIM(u, v) = \frac{1}{M}\sum_{i=1}^{M}\Big(u(i), v(i)\Big), \tag{24}$$

where M is the number of local windows in the image while $MSSIM \in [0, 1]$. Higher MSSIM indicates better structural similarity between two images.

Signal-to-noise ratio (SNR) is also applied to determine the visual quality of restoration of the restored image and is defined as:

$$SNR = 10log_{10} = \frac{\|u - u_0\|}{\|n - n_0\|}, \tag{25}$$

where u and n indicate the true image and noise, while u_0 and n_0 describe their mean values in the image domain Ω. Repeatedly, the greater SNR value leads to better restoration results.

The stopping criteria for iterations in meshless scheme M2 is given by the following equation

$$\frac{\|z^{(k+1)} - z^{(k)}\|}{z^{(k)}} \leq \epsilon, \tag{26}$$

where ϵ shows the maximum acceptable error with $\epsilon = 10^{-4}$. In meshless scheme M2, Multiquadric radial basis function (MQ-RBF) is selected as a basis function. The formula for

(a) (b) (c) (d)

FIGURE 2. De-noised results on Cameraman; (a) Original image; (b) Noisy image with $\sigma 1 = 15$; (c) Resultant image by method M1; (d) Resultant image by method M2.

(a) (b) (c) (d)

FIGURE 3. Obtained results on Moon; (a) Original image; (b) Noisy image with $\sigma 1 = 18$; (c) Restored image by using method M1; (d) Restored image by using method M2.

(a) (b) (c) (d)

FIGURE 4. Experimental results on Peppers; (a) Original image; (b) Noisy image with $\sigma 1 = 22$; (c) Obtained image by using M1; (d) Obtained image by using M2.

(a) (b) (c) (d)

FIGURE 5. Experimental results on house; (a) Original image; (b) Noisy image with $\sigma 1 = 24$; (c) Obtained image by using M1; (d) Obtained image by using M2.

MQ-RBF for each point (x_i, y_j) is defined by the given equation.

$$\phi_j(x, y) = \sqrt{c^2 + r_j^2} = \sqrt{c^2 + (x - x_j)^2 + (y - y_j)^2},$$

where $r_j = \sqrt{(x - x_j)^2 + (y - y_j)^2}$.

Experiment 1: In experiment 1, three real images 'Cameraman', 'Moon', 'Peppers', and 'House' are applied and tested on mesh-based scheme M1 and proposed meshless scheme M2 for Gaussian noise (Gaussian noise with mean value zero and standard deviation $\sigma 1$) with standard deviation of $\sigma 1 = 15$, $\sigma 1 = 18$, $\sigma 1 = 22$, and $\sigma 1 = 24$, respectively. All the four images are given in Figures 2, 3, 4, and 5, respectively. In all the three Figures mentioned for the three real images, (a) and (b) represent the true and degraded images while (c) and (d) described the resultant images by algorithms M1 and M2. In each case, it can be observed that the quality of the reconstructed images obtained using M2 is far better than the image quality of the restored images achieved utilizing method M1, without degrading the intrinsic jumps in the clean data, and also preserve the edges quite well due to the applications of DTV filter and the meshless applications due to the meshless characteristics of MQ-RBF approximation applied to the smooth of DTV based nonlinear

TABLE 1. The PSNR, SSIM values and the statistical iterations numbers (Iters) and run time (Cpu time) for computation.

Image	Size	Scheme M1				Scheme M2			
		PSNR	MSSIM	Iter	Time	PSNR	MSSIM	Iter	Time
Cameraman	360^2	32.80	0.8022	28	17.29	33.60	0.8941	18	12.65
Moon	360^2	33.70	0.7936	34	20.31	34.70	0.7874	21	14.89
Peppers	360^2	34.09	0.8110	39	23.11	35.50	0.9007	25	16.51
House	360^2	29.70	0.7411	40	29.49	30.17	0.8791	27	16.22
Ring	360^2	30.75	0.7860	26	20.85	32.11	0.8899	17	11.57
Lena	360^2	32.30	0.8447	25	19.30	33.10	0.9197	15	12.43
Bird	360^2	30.11	0.7971	36	22.72	30.96	0.8682	23	16.87
Bridge	360^2	28.76	0.8407	32	29	29.27	0.9097	19	17.33
Peppers (color)	360^2	34.70	0.841	41	38.2	35.40	0.9239	33	31.83
Sanada (color)	360^2	35.40	0.7980	43	43.27	36.40	0.9117	37	35.11
Man (color)	360^2	32.12	0.77087	48	41.45	32.97	0.8927	35	30.98
Rose (color)	360^2	36.11	0.8102	50	44.95	36.94	0.9004	38	37.7
Figure 15		26.00	0.9000	30	24.25	29.19	0.9511	30	14.97

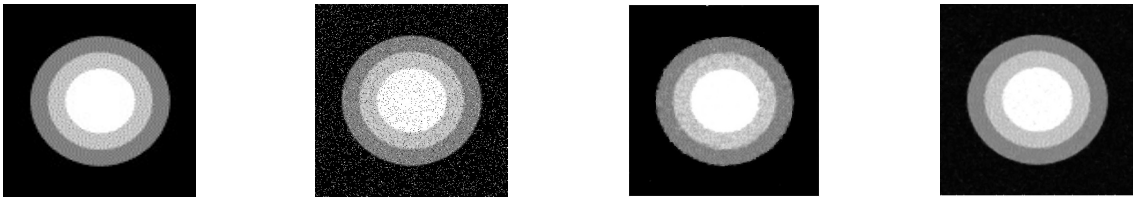

(a) (b) (c) (d)

FIGURE 6. Restored results on Ring; (a) True image; (b) Noisy image with $\sigma 2 = 0.10$; (c) De-noised image by scheme M1; (d) De-noised image by scheme M2.

(a) (b) (c) (d)

FIGURE 7. Reconstructed results on Lena; (a) True image; (b) Noisy image with $\sigma 2 = 0.11$; (c) Restored image by M1; (d) Restored image by M2.

equation. The PSNR and SSIM values for the three images in this experiment are listed in Table 1. The bigger the PSNR and SSIM value results in good restoration performance. Thus, it can be seen from Table 1, that the PSNR and SSIM values utilized by using M2 are greater than that of M1 in each case which represents the good restoration performance of M2. The number of iterations required for convergence and the computational time obtained by the meshless scheme M2 is also smaller than of method M1 in each case which shows the accelerated denoising performance of introduced meshless scheme M2 over mesh-based scheme M1 because of the meshless application of the lack of dependency on a mesh or integration procedure connected with MQ-RBF for the solution of DTV based nonlinear restoration equation. The values of the two parameters i.e. (shape parameter c, the fitting parameter λ) selected for the M2 for the three test images 'Cameraman', 'Moon', and 'Peppers' in this experiment are (0.45, 0.315), (0.47, 0.274), (0.50, 0.259), and (0.52, 0.254), and respectively. The shape parameter c plays an essential role in image restoration in proposed meshless scheme M2 [32]. The **fminbnd** Matlab function has been used in this experiment to get the best value of $c \in (c_{min}, c_{max})$ for the best restoration results shown in Table 1. In this test, $c_{min} = 0.37$ and $c_{max} = 0.79$ are chosen.

Experiment 2: In this experimental test 2, the restoration results for two algorithms M1 and M2 are check on artificial and real images 'Ring', 'Lena', 'Bird', and 'Bridge' having salt and paper noise (slat and paper noise with mean value zero and standard deviation $\sigma 2$) that are shown in Figures 6, 7, 8, and 9, respectively. The noise levels in this test for 'Ring', 'Lena', 'Bird', and 'Bridge' are set to $\sigma 2 = 0.08$, $\sigma 2 = 0.17$, $\sigma 2 = 0.21$, and $\sigma 2 = 0.24$, respectively. Again for each case, the performance of the restored images and edge preservation property by Kansa method M2 (shown in Figures (6(d), (7(d), (8(d), and (9(d)) are much better than of traditional method M1 (shown in Figures (6(c), (7(c)), (8(c)) and (9(c), respectively). The PSNR and SSIM values, number of iterations, and CPU times for this experiment are also listed in Table 1, which shows better performance of the proposed algorithm M2 over algorithm

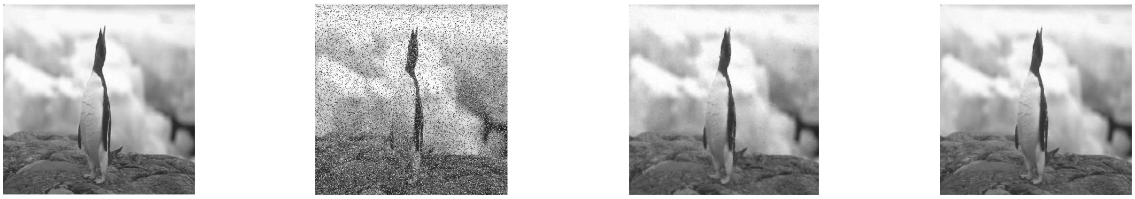

(a) (b) (c) (d)

FIGURE 8. Reconstructed results on bird; (a) True image; (b) Noisy image with $\sigma 2 = 0.11$; (c) Restored image by M1; (d) Restored image by M2.

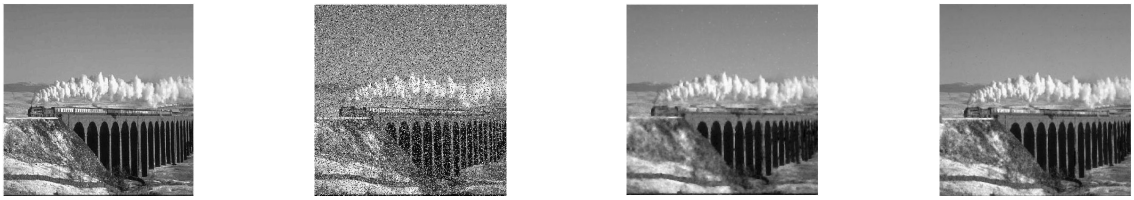

(a) (b) (c) (d)

FIGURE 9. Reconstructed results on bridge; (a) True image; (b) Noisy image with $\sigma 2 = 0.11$; (c) Restored image by M1; (d) Restored image by M2.

(a) (b) (c) (d)

FIGURE 10. De-noised results on Color Peppers; (a) True image; (b) Degraded image with $\sigma 1 = 19$; (c) Reconstructed image by method M1; (d) Reconstructed image by method M2.

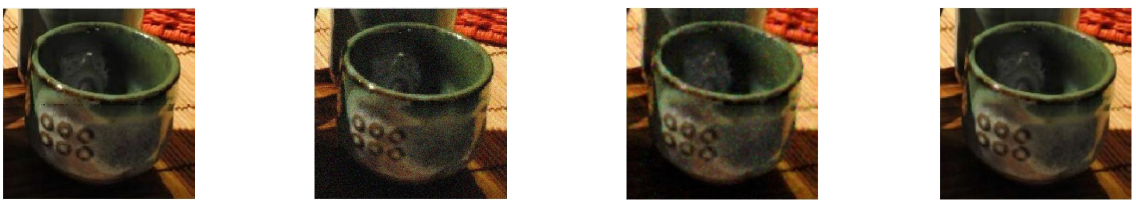

(a) (b) (c) (d)

FIGURE 11. Reconstructed results on Color Sanada; (a) True image; (b) Noisy image with $\sigma 1 = 22$; (c) Obtained image by M1; (d) Obtained image by M2.

M1 because of meshless properties of MQ-RBF used in M2. Again, this experiment demonstrates the high efficiency of M2 compared to M1 regarding image restoration (PSNR, SSIM values) and faster convergence (iterative numbers in computational time (CPU Time)). The best experiential values of parameters i.e. shape parameter c and fitting parameter iλ used in M2 for the two images 'Ring', 'Lena', 'Bird', and 'Bridge' are $(0.44, 0.413)$, $(0.47, 0.396)$, $(0.48, 0.387)$ and $(0.49, 0.371)$, respectively. Again, **fminbnd** Matlab function has been utilized to obtain the good value of $c \in (c_{min}, c_{max})$ for the best image recovery result shown in Table 1. In this test, $c_{min} = 0.37$ and $c_{max} = 0.79$ are selected.

Experiment 3: In the third experiment, the two schemes M1 and M2 are tested on 3D coluor images 'Peppers', 'Sanada', 'Man', and Roses' containing Gaussian noises that are displayed in Figures 10, 11, 12, and 13, respectively. It can be observed from Figure 10, 11, 12, and 13 that the proposed scheme M2 can successfully remove the noise without much smearing of the sharp edges from the two images 'Peppers', 'Sanada', 'Man', and 'Roses', (shown in Figures (10(d), (11(d), (12(d), and (13(d)), respectively, which only show the good image restoration performance (PSNR, SSIM values), reducing the staircase effect but also indicates the edge enhancement and texture preservation character of proposed method M2 over method M1 (shown in Figures (10(c), (11(c), (12(c), and (13(c)), respectively) even on color images due to the effectiveness of MQ-RBF Kansa method M2 for the smooth solution of complex images. Furthermore, it can be observed that M2 produces better purity of colors in

(a) (b) (c) (d)

FIGURE 12. Reconstructed results on Color Man; (a) True image; (b) Noisy image with $\sigma 1 = 22$; (c) Obtained image by M1; (d) Obtained image by M2.

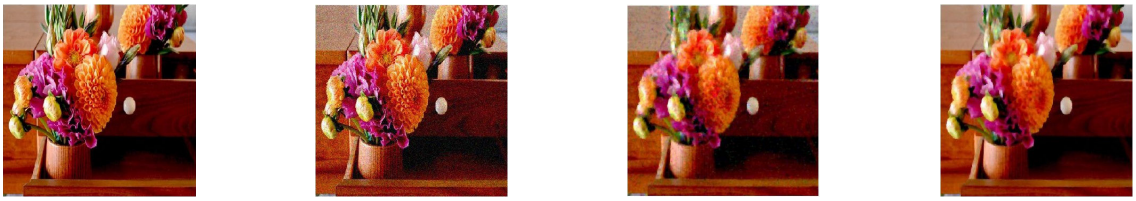

(a) (b) (c) (d)

FIGURE 13. Reconstructed results on Color Rose; (a) True image; (b) Noisy image with $\sigma 1 = 22$; (c) Obtained image by M1; (d) Obtained image by M2.

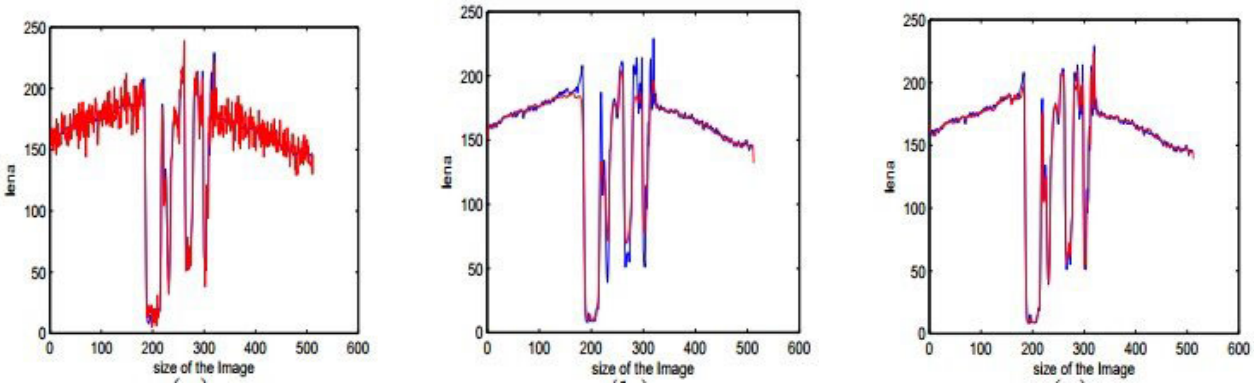

(a) (b) (c)

FIGURE 14. Comparison of 121^{th} lines of Lena original image, the noisy image with additive noise, and restored images using algorithms M1and M2. (a) Comparison of true and noisy lines; (b) Original and restored lines comparison using M1; (c) Original and reconstructed lines comparison using M2. The blue line shows the true image line while the red line indicates the reconstructed image line.

homogeneous regions and sharper boundaries in between for two images than M1 as shown in Figures (10(d), (11(d), (12(d) and (13(d), respectively. The PSNR and SSIM values, number of iterations and CPU times of this experiment are shown in Table 1. (0.52, 0.439), (0.55, 0.429), (0.55, 0.429) and (0.56, 0.426) are the values of the parameters i.e. shape parameter c and fitting parameter λ used in proposed method M2 for two colours images 'Peppers', 'Sanada', 'Man', and 'Roses', respectively. The **fminbnd** Matlab function is used to get the best restoration result for the best selected value of c.

Experiment 4: The homogeneity and preservation (or loss) are analyzed for the two schemes M1 and M2 applied on 'Lena'. To achieve this aim, the 121^{th} line of true image compared with degraded and obtained images, which are given in Fig. 14. It can be seen from Fig. 14 that the lines obtained by meshless scheme M2 is better than what is obtained using scheme M1.

Experiment 5: Figure 15 presents the SSIM and PSNR curves of the traditional mesh-based scheme M1 and the proposed meshless scheme M2 after different iterations. The convergence rate of the meshless scheme M2 is faster than the mesh-based scheme M1. Another judgment from Figure 15 is that the SSIM and PSNR values of the meshless scheme M2 are higher than the values of the mesh-based scheme M1. The comparison results confirm that the proposed method M2 reproduces the source image better and gives higher SSIM and PSNR in less iterations. The calculation time along with iterative numbers of these two methods with the same level SSIM and PSNR are recorded in Table 1.

V. COMPARSION WITH OTHER SCHEMES

A. COMPARISON WITH ROF SCHEME (M3)

The primary TV-based model for image denoising possessing additive noise was introduced by Rudin-Osher-Fatemi (ROF) [11]. This scheme performed good results in terms

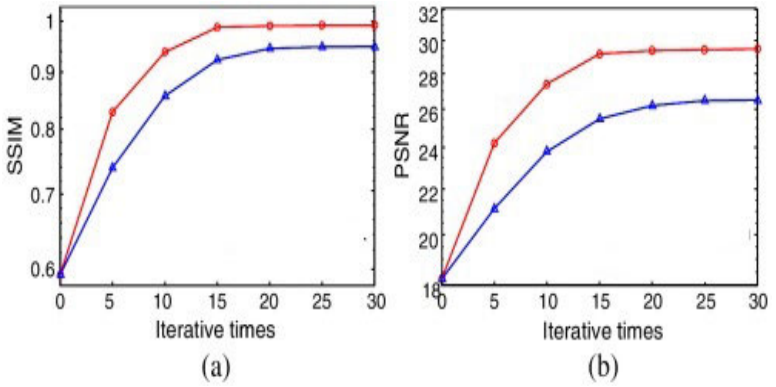

FIGURE 15. SSIM and PSNR converge curves of two iterative schemes M1 and M2. The blue line presents convergence scheme M2 while the red line indicates the convergence proposed meshless M2.

of image restoration on 2D grayscale images. The TV-based minimization functional applied by ROF for the model (1) is presented as follows.

$$\widehat{z} = \min_{z} E(z) = \int_{\Omega} |\nabla z| dxdy + \frac{\lambda}{2}\|z - z^0\|_2^2, \qquad (27)$$

with $|\nabla z| = \sqrt{z_x^2 + z_y^2}$, where the two terms in equation (23) are called the regularization term and data fitting terms, while λ is the scale parameter which controls the similarities between the denoised and the original images which normally depends on upon the noise level. The resultant Euler Lagrange PDE received from model (23) is determined as below.

$$\frac{\partial}{\partial x}\left(\frac{z_x}{\sqrt{z_x^2 + z_y^2}}\right) + \frac{\partial}{\partial y}\left(\frac{z_y}{\sqrt{z_x^2 + z_y^2}}\right) + \lambda(z - z_0) = 0, \quad (28)$$

in Ω, where $\frac{\partial z}{\partial n} = 0$ on $\partial\Omega = \Omega$. The time marching PDE from equation (24) is re-written as follow;

$$\frac{\partial z}{\partial t} = \frac{\partial}{\partial x}\left(\frac{z_x}{\sqrt{z_x^2 + z_y^2}}\right) + \frac{\partial}{\partial y}\left(\frac{z_y}{\sqrt{z_x^2 + z_y^2}}\right) + \lambda(z - z_0), \quad (29)$$

for $t > 0$, and $(x, y) \in R$. The numerical solution of the PDE equation (25) has been discussed and explained in [11].

B. COMPARISON WITH DTV-FILTERING BASED SCHEME (M4)

Osher and Shen [53] introduced a different DTV filter-based model for image reconstruction having additive noise. The energy functional of model (1) by [53] is provided as below.

$$\min_{z} E(z) = \sum_{\beta_1 \in \Omega} \varphi \left\| \nabla_p z_{\beta_1} \right\|_{\alpha} + \frac{\lambda}{2} \sum_{\beta_1 \in \Omega} \left\| z_{\beta_1} - z^0_{\beta_1} \right\|_{\Omega}^2, \quad (30)$$

where $\varphi(x)$ is a simple function and $\varphi(x) = x^{2-q}$ for $0 \le q \le 2$. The equation (26) results in given restoration equation.

$$(z_{\beta_1} - z_{\beta_2})\left[\frac{\varphi'\|\nabla_p z_{\beta_1}\|_{\alpha}}{\|\nabla_p z_{\beta_1}\|_{\alpha}} + \frac{\varphi'\|\nabla_p z_{\beta_2}\|_{\alpha}}{\|\nabla_p z_{\beta_2}\|_{\alpha}}\right] + \lambda(z_{\beta_1} - z^0_{\beta_1}) = 0. \quad (31)$$

The nonlinear recovery system of equations from equation (26) is given as follows.

$$\left[\lambda + \sum_{\beta_1 \in \Omega} \omega_{\beta_1\beta_2(z)}\right] z_{\beta_1} - \sum_{\beta_2 \in \Omega} \omega_{\beta_1\beta_2(z)} z_{\beta_2} = \lambda z^0_{\beta_1}. \quad (32)$$

for all $\beta_1 \in \Omega$. The authors used the Gauss-Jacobi scheme to resolve the system of nonlinear equation (28) which is reproduced as below.

$$z^{n+1}_{\beta_1} = \sum_{\beta_2 \in \Omega} \left(\frac{\omega_{\beta_1\beta_2(z^n)}}{\lambda + \omega_{\beta_1\beta_2(z^n)}}\right) z^n_{\beta_1} + \sum_{\beta_2 \in \Omega} \left(\frac{\lambda}{\lambda + \omega_{\beta_1\beta_2(z^n)}}\right) z^0_{\beta_1}, \quad (33)$$

where

$$\omega_{\beta_1\beta_2(z)} = \frac{\varphi'\|\nabla_p z_{\beta_1}\|_{\alpha}}{\|\nabla_p z_{\beta_1}\|_{\alpha}} + \frac{\varphi'\|\nabla_p z_{\beta_2}\|_{\alpha}}{\|\nabla_p z_{\beta_2}\|_{\alpha}}.$$

For further details, see [53].

Experiment 6: In this analysis, the recommended collocation scheme M2 is compared to schemes M3 and M4 for two real images 'Lena' and 'Peppers' holding additive Gaussian noises. Repeatedly, from the experimental outcomes, we can see that M2 is better in image recovery (PSNR), iterative numbers, and time of computation (CUP time) corresponded with schemes M3 and M4. Those reconstructed results are displayed in Figures 16, 17, and Table 2, respectively. Consequently, this analysis confirms the effectiveness of the meshless MQ-RBF applications used in M2.

C. A NEW METHOD FOR IMAGE RESTORATION IN THE PRESENCE OF IMPULSE NOISE (M5)

Yuan and Ghanem [54] has introduced a new scheme for a TV-based model for the removal of impulsive noise from the given image data and delivered good restoration results. The minimization functional for this model is defined as below.

$$arg \min_{0 \le u,v \le} \langle 1, 1 - v\rangle + \lambda\|\nabla u\|_{p,1}$$
$$s.t\ v \odot |o \odot (Ku + b)| = 0. \quad (34)$$

(a) (b) (c) (d) (e)

FIGURE 16. Obtained results on Lena; (a) True image; (b) Noisy image with $\sigma 1 = 22$; (c) Resultant image by M3; (d) Resultant image by M4; (e) Resultant image by proposed method M2 ($c = 0.433$, $\lambda = 0.511$).

(a) (b) (c) (d) (e)

FIGURE 17. Reconstructed results on Peppers; (a) True image; (b) Noisy image with $\sigma 1 = 20$; (c) Resultant image by M3; (d) Resultant image by M4; (e) Resultant image by proposed method M2 ($c = 0.515$, $\lambda = 0.432$).

TABLE 2. Comparison Of the two algorithms M1 and M2 regarding PSNR values, iterative numbers, and Cpu-times.

Image	Size	Method M3			Method M4			Proposed Method M2		
		PSNR	Iterations	CPU Times(s)	PSNR	Iterations	CPU Times(s)	PSNR	Iterations	CPU Times(s)
Peppers	360^2	30.21	45	34.12	30.48	36	29.01	31.03	29	23.12
Sanada	360^2	32.70	38	31.45	32.97	33	26.27	33.40	27	20.89
Man	360^2	28.22	40	33.19	28.89	44	28.76	30.02	38	21.85
Rose	360^2	34.01	54	39.47	34.50	46	32.26	35.67	39	27.12

where u describes the clean image, b is noisy or blurred image, K denotes the linear operator, a and b are the noise vectors, $\odot$ shows the elementwise product, and p is a parameter such that $p = 1$ for isotropic TV model and $p = 2$ for anisotropic TV model. Here, we choose $K = 1$. The contributors utilized the proximal ADMM strategy, which iteratively renewed the primal and dual variables of the augmented Lagrangian function of equation (34). For any auxiliary $x \in \Re^{2n}$ and $y \in \Re^n$, equation (34) can be rewritten as

$$\begin{aligned} &arg \min_{0\le u,v\le} \langle 1, 1-v\rangle + \lambda\|\nabla u\|_{p,1} \\ &s.t \quad \nabla u = x, \quad Ku - b = y, \quad v \odot o \odot |y| = 0. \end{aligned} \tag{35}$$

Similarly, for $\pounds_\beta : \Re^n \times \Re^n \times \Re^{2n} \times \Re^n \times \Re^{2n} \times \Re^n \longrightarrow \Re$ be the augmented Lagrangian function of (35).

$$\begin{aligned} &\pounds_\beta(u, v, x, y, \xi, \zeta, \pi) \\ &:= \langle 1, 1-v\rangle + \lambda\|\nabla u\|_{p,1} \\ &\quad +\langle \nabla u - x, \xi\rangle + \frac{\beta}{2}\|Ku - x\|^2 + \langle \nabla u - b - y, \zeta\rangle \\ &\quad +\frac{\beta}{2}\|\nabla u - b - y\|^2 + \langle v \odot o \odot |y|, \pi\rangle + \frac{\beta}{2}\|v \odot o \odot |y|\|^2, \end{aligned}$$

where ξ, ζ, and π represent the Lagrange multipliers connected with the constrains $v \odot o \odot |y| = 0$, respectively, while $\beta > 0$ is the penalty parameter. For further details, the readers are refereed to [54].

D. HIGHLY ACCURATE IMAGE RECONSTRUCTION FOR MULTIMODEL NOISE SUPPRESSION USING SEMISUPERVISED LEARNING ON BIG DATA (M6)

Yin *et al.* [55] established a new model and scheme to remove the impulse noise from the image data. The model for reconstructed image f for each pixel x at the i^{th} position is given by the given equation.

$$f(x_i) = \theta_0 g(x_i) + \theta_1 l(x_i) + \theta_1 s(x_i) + \epsilon(x_i), \tag{36}$$

where θ_0, θ_1, and θ_2 express unknown linear coefficients. $\epsilon(\cdot)$ determines the random-error map of the model, applying the Gaussian density $\epsilon(x_i) \sim G(0, \sigma^2)$. The optimization procedure based on Sparsity, Density and Multimodality has been used by the authors to impulsive noise from noisy image. By employing the semisupervised cost function ϕ, the

model (36) is redefined as

$$f^* = arg\min_{f}\{\phi\}. \tag{37}$$

The effect of the above cost function is to divide the model into three different stages for the solution.

In the first stage, ϕ is used to denoise the image corrupted by high-density noise. The functions ϕ_1, ϕ_2, and ϕ_3 are given as follows.

$$\phi_1(f) = \sum_{\forall x_i \in x^{nf}} \left|x_i - f(x_i)\right|. \tag{38}$$

$$\phi_2(f) = \sum_{\forall x_i \in x^{n}} \gamma_{i,j}\left(\left|f(x_i) - f(x_j)\right|\right). \tag{39}$$

$$\phi_3(f) = \left|\frac{1}{w_1}\sum_{\forall x_i \in x^{nf}} x_i - \frac{1}{w_2}\sum_{\forall x_i \in x} f(x_i)\right|. \tag{40}$$

On the second stage, the number of images considered to be noise-free in the large-volume image set D is limited. Correspondingly, images identified to be clean in the training set are extremely sparse. In this situation, the fourth term of ϕ_4 is given as under.

$$\phi_4(f) = \sum_{\forall x \in D^n}\sum_{\forall x_i \in x}\left|x_i - f(x_i)\right|. \tag{41}$$

In the third stage, the images in the large-volume image set D may be contaminated with various types of noises. Accordingly, the aforementioned property of average intensity shows that the average intensity of the reconstructed image set is similar to that of the clean pixels in the corrupted image set. This is shown in the fifth term of the stated cost function ϕ_5 is given as follows.

$$\phi_5(f) = \left|\frac{1}{w^3}\sum_{\forall x \in D}\sum_{\forall x_i \in x^{nf}} x_i - \frac{1}{w^3}\sum_{\forall x \in D}\sum_{\forall x_i \in x} xf(x_i)\right|. \tag{42}$$

So the combination of all the equations results in total cost function and is given by the formula.

$$\phi(f) = \phi_1(f) + \lambda\phi_2(f) + \phi_3(f) + \phi_4(f) + \phi_5(f). \tag{43}$$

For more information, see [55].

E. WEIGHTED COUPLE SPARSE REPRESENTATION WITH CLASSIFIED REGULARIZATION FOR IMPULSE NOISE REMOVAL (M7)

Chen *et al.* [56] proposed a model for image restoration having impulsive noise which is given as under.

$$\begin{aligned}(\hat{a}, \hat{D}, \hat{Y}) = arg\min_{a,D,Y}\Bigg\{&\sum_{i,j}\frac{1}{2}\left\|R_{i,j}W \otimes \left(R_{i,j}X - Da_{i,j}\right)\right\|_2^2 \\ &+ \sum_{i,j}\frac{1}{2}\left\|R_{i,j}(I-W) \otimes \left(R_{i,j}Y - Da_{i,j}\right)\right\|_2^2 \\ &+ \frac{\lambda_1}{2}\left\|W \otimes (Y-X)\right\|_2^2 + \lambda_2\left\|\bar{W} \otimes (Y-X)\right\|_1\Bigg\}, \\ s.t \quad &\|a_{i,j}\|_0 \le L,\end{aligned} \tag{44}$$

where X shows the corrupt image, W is the weighted matrix generated by a noise detector, $D \in R^{n\times K}(n < K)$ is a redundant dictionary,$R_{i,j}$ matrix that is used to extract the $(i,j)^{th}$ $\sqrt{n}\times\sqrt{n}$ patch from the image, a is the representation coefficient expected to be sparse, and L is the sparse ratio. By alternating minimization method is utilized to solve the model (44) and is given by the given equation.

$$\begin{aligned}\hat{Y} = arg\min_{Y,a}\Bigg\{&\sum_{i,j}\frac{1}{2}\left\|R_{i,j}(I-W) \otimes \left(R_{i,j}Y - Da_{i,j}\right)\right\|_2^2 \\ &+ \sum_{i,j}\frac{1}{2}\left\|R_{i,j}W \otimes \left(R_{i,j}X - Da_{i,j}\right)\right\|_2^2 \\ &+ \frac{\lambda_1}{2}\left\|W \otimes (Y-X)\right\|_2^2\Bigg\}, \quad s.t \quad \|a_{i,j}\|_0 \le L. \\ s.t\ &\|a_{i,j}\|_0 \le L.\end{aligned} \tag{45}$$

Similarly, the resultant restoration image can be calculated pixel by pixel by the given formula.

$$y_{i,j} = \begin{cases} x_{i,j} & if\ w_{i,j} = 1 \\ \dfrac{z_{i,j}}{m_{i,j}} & if\ w_{i,j} = 0 \\ . \end{cases}$$

For more information, the researchers are refereed to [c] [56].

Experiment 7: In this experiment, we examine the reconstruction performance of the suggested meshless methods M2 with the latest state-of-art schemes M5, M6, and M7, respectively.

In the first example, the two schemes M2 and M5 are examined concerning image restoration performance on the real images 'peppers' and 'Lena' images containing impulsive noise for the same high noise levels and parameter values as chosen in [54]. All the reconstruction results are given in Figures 18 and 19, and displayed in Table 3, respectively. We can observe from the Figures 18 and 19, and Table 3, that the visual quality of image recovery (PSNR values) performance of the proposed meshless algorithm M2 is far better than scheme M5 concerning image restoration (PSNR values), minimization of staircase effect, textures and recovering edges. The importance of M2 for best reconstruction outcomes than M5 is due to the MQ-interpolation process which is responsible for edges preservation. Also due to the lack of dependence on a mesh or integration procedure and the Euclidian distance between a noisy pixel and other non-noisy pixel values applications used in the proposed scheme M2 are responsible for the unique smooth solution which results for qualified restoration results.

In the second example, the recommended scheme M2 is further examined with scheme M6 for the same high noise levels, image size, and parameters picked in [55] and are exhibited in Figures 20,21,22, and 23, and Table 4, respectively. In this illustration, repeatedly the suggested algorithm M2 produces more reliable restoration results than algorithm M6 due to the meshless utilization as discussed in the

(a) (b) (c) (d)

FIGURE 18. Restored results on Lena; (a) Original image; (b) Noisy image with salt and paper noise $\sigma 2 = 50$; (c) Reconstructed image by M5; (d) Reconstructed image by M2.

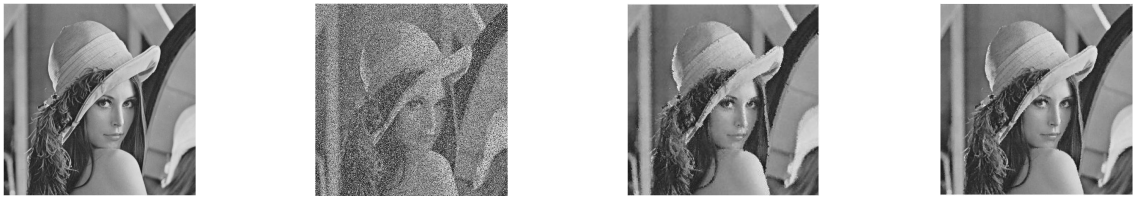

(a) (b) (c) (d)

FIGURE 19. Obtained results on lena; (a) True image; (b) Noisy image with 50 percent impulse noise; (c) Resultant image by M5; (d) Resultant image by M2.

TABLE 3. Comparison of the two algorithms regarding PSNR.

Noise	Image	Size	Algorithm M5	Algorithm M2
			PSNR	PSNR
Impulsive Noise				
50	Lena	512^2	12.69	13.02
90	Lena	512^2	5.55	5.78
50	Cameraman	512^2	12.56	12.91
90	Cameraman	512^2	3.91	4.11
Salt and Paper Noise				
50	Lena	512^2	20.10	20.75
90	Lena	512^2	11.27	11.71
50	Cameraman	512^2	22.04	22.47
90	Cameraman	512^2	11.34	11.65

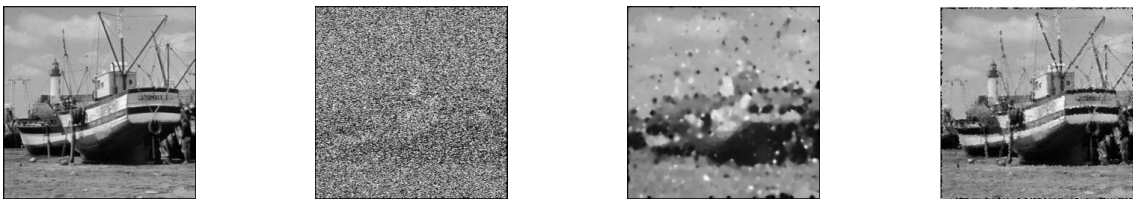

(a) (b) (c) (d)

FIGURE 20. Obtained results on boat; (a) Real image; (b) Noisy image with 80 percent impulsive noise; (c) Reconstructed image by M6; (d) Reconstructed image by M2.

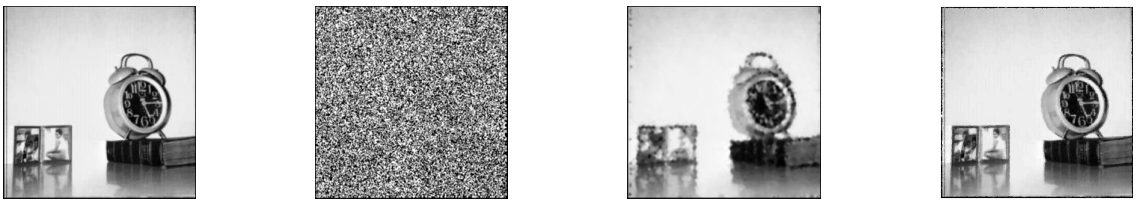

(a) (b) (c) (d)

FIGURE 21. Denoised results on clock; (a) Original image; (b) Noisy image with 90 percent impulsive noise; (c) Restored image by M6; (d) Restored image by M2.

above-mentioned case first. More importantly, the homogeneous regions in the color images are also recovered sharply in this experiment.

In the third example, again the reconstruction performance of the meshless scheme M2 is excellent over scheme M7 [56] in image restoration completion presented in Figures 24, 25,

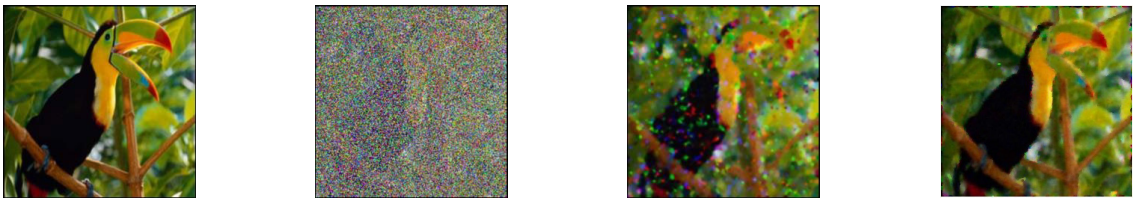

(a) (b) (c) (d)

FIGURE 22. Restored results on color bird; (a) True image; (b) Noisy with 80 percent impulsive noise; (c) Denoised image by M6; (d) Obtained image by M2.

(a) (b) (c) (d)

FIGURE 23. Reconstructed results on color barbara; (a) True image; (b) Noisy image with 90 percent impulsive noise; (c) Restored image by M6; (d) Restored image by M2.

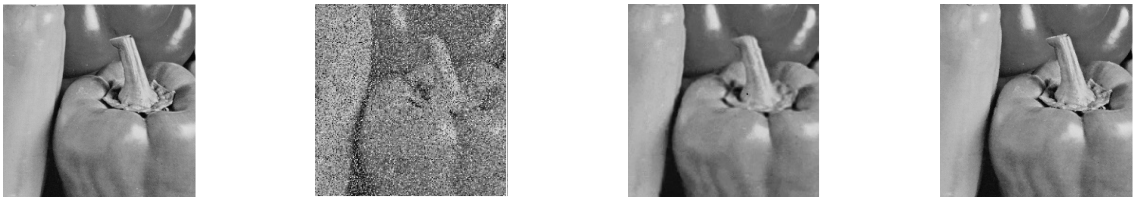

(a) (b) (c) (d)

FIGURE 24. Obtained results on a part of Peppers; (a) True image; (b) Noisy image with with 50 percent impulsive noise; (c) Denoised image by M7; (d) Denoised image by M2.

TABLE 4. Comparison of the two algorithms regarding PSNR.

Image	Szie	Noise (SPN)	Method M6	Method M2
			PSNR	PSNR
Lake (grayscale)	256^2	80	22.41	22.79
Clock (grayscale)	256^2	90	23.89	24.17
Boat (grayscale)	256^2	80	18.60	18.96
Butterfly (color)	256^2	80	22.75	23.09
Woman (color)	256^2	90	22.26	22.60
Bird (color)	256^2	80	18.54	18.89

TABLE 5. Comparison of the two algorithms regarding PSNR.

Image	Szie	Noise (SPN)	Method M7		Method M2	
			PSNR	SSIM	PSNR	SSIM
Barbara	256^2	50	24.37	0.7040	24.59	0.8145
Barbara	256^2	80	23.08	0.6583	23.24	0.7840
Peppers	256^2	50	30.55	0.8483	30.77	0.9011
F16	256^2	80	28.89	0.8788	29.06	0.9020
Boat	256^2	80	26.68	0.7801	26.85	0.8122
House	256^2	80	35.05	0.9385	35.20	0.9509

and 26, and displayed in Table 5, respectively. Repeatedly the meshless applicability of meshless scheme makes the meshless scheme M2 more active in image restoration in all perspectives than M7.

To summarize this experiment, we can observe that the achievements of image restoration concerning image restoration (PSNR values), minimization of staircase effect, textures and recovering edges of the recommended meshless scheme M2 is stable than M5, M6, and M7 due to the meshless application of MQ-RBF approach used in proposed method M2.

Experiment 8: In this experiment, we have implemented the recommended algorithm M2 for varying additive Gaussian noise levels on 15 randomly selected images from the Berkeley images database BSD500 for image restoration in terms of the average PSNR SSIM values. All the information concerning the average PSNR and SSIM values is recorded in Table 6.

VI. SENSITIVITY ANALYSIS OF PARAMTERS

In this section, we will briefly discuss the selection of shape parameters shape parameter c and fitting parameter λ used in the proposed meshless scheme and their impact on image restoration. Since from experimental results, we can say the best-selected value chosen in meshless method M2 is quite complicated. Nevertheless, its best-selected values are adjusted and tuned according to the noise variance, image size, etc. It has been noticed that the range of values allowed is: $c \in [0.37,0.79]$ and $\lambda \in [0.245,0.502]$, for natural and artificial images. This shows that both the parameters c and λ

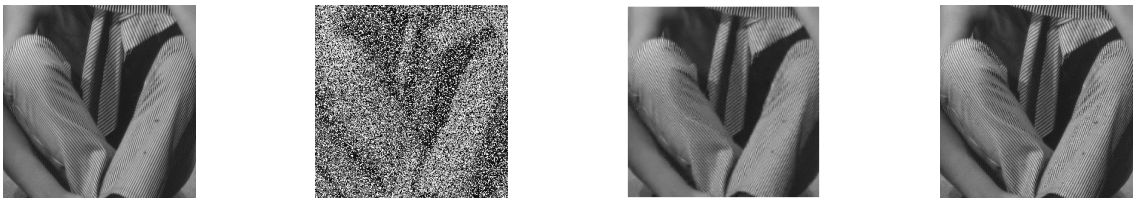

(a) (b) (c) (d)

FIGURE 25. Reconstructed results on a part of barbara; (a) True image; (b) Noisy image with 50 percent impulsive noise; (c) Obtained image by M7; (d) Obtained image by M2.

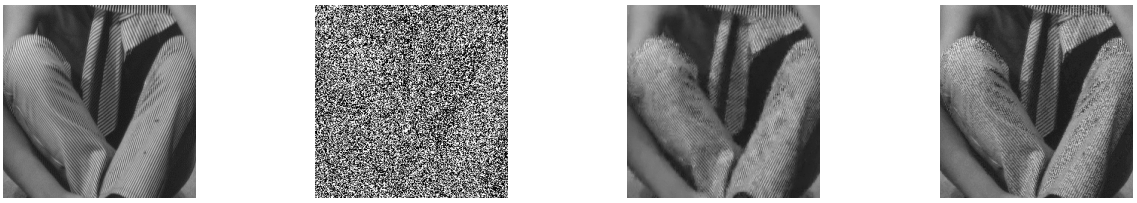

(a) (b) (c) (d)

FIGURE 26. Denoised results on a part of barbara; (a) True image; (b) Noisy image with 80 percent impulsive noise; (c) Obtained image by M7; (d) Obtained image by M2.

TABLE 6. The average SSIM and PSNR values of 15 images chosen from the Berkeley image database BSD500 by proposed meshless scheme M2 for different additive Gaussian noise levels.

Image ID	55%		60%		65%		70%	
	PSNR	SSIM	PSNR	SSIM	PSNR	SSIM	PSNR	SSIM
3063	27.10	0.853	25.98	0.792	25.47	0.742	24.94	0.712
43051	28.38	0.873	27.49	0.814	27.20	0.781	26.69	0.759
393035	23.76	0.801	23.07	0.772	22.59	0.742	22.30	0.719
334024	24.70	0.812	24.06	0.785	23.73	0.751	23.42	0.716
188063	25.83	0.805	25.20	0.779	24.80	0.747	24.54	0.712
374020	25.46	0.790	25.03	0.762	24.65	0.735	24.34	0.702
385028	23.47	0.821	22.80	0.791	22.31	0.761	21.92	0.739
219090	26.65	0.847	26.30	0.8191	25.75	0.792	25.27	0.757
119082	28.74	0.831	28.26	0.8041	27.74	0.784	27.21	0.743
301007	23.18	0.793	22.71	0.774	22.09	0.769	21.61	0.731
12003	25.03	0.809	24.52	0.781	24.04	0.762	23.46	0.725
117025	24.05	0.798	23.44	0.764	22.97	0.749	22.39	0.732
103078	25.99	0.852	25.31	0.827	24.89	0.795	24.43	0.761
120003	26.30	0.852	25.61	0.810	24.80	0.783	24.29	0.754
223060	23.51	0.829	22.80	0.803	22.29	0.789	21.83	0.758
Average PSNR and SSIM	25.48	0.823	24.84	0.792	24.35	0.765	23.91	0.735

TABLE 7. Comparison in percentage change in PSNR value of real 'Cameraman' image of size (360^2) for percentage increase in best selected values of parameters used in M2.

Image	40 % (↑)			70% (↑)		
	c	λ	PSNR	c	λ	PSNR
Cameraman	0.63	0.1890	2.39(↓)	0.77	0.2295	4.17(↓)

TABLE 8. Comparison in percentage change in PSNR value of real 'Cameraman' image of size (360^2) for percentage decrease in best selected values of parameters used in M2.

Image	40 % (↓)			70% (↓)		
	c	λ	PSNR	c	λ	PSNR
Cameraman	0.27	0.0810	2.67(↓)	0.14	0.0405	5.11(↓)

used in M2 are valuable for enhancing the denoising performance. Likewise, the range of iterations to improve the PNSR results is [20, 90]. Thus, the availability of information about the uncertainty of the denoising result on the user-chosen parameters is helpful to avoid incorrect decisions. For briefness, Tables 7 and 8 shall be denoted by

1. (•)% increase $-\uparrow$, (•)% decrease $-\downarrow$.
2. For instance (0.22) $\downarrow$ denotes 0.22% decrease in PSNR.
3. (0.27) $\uparrow$ denotes 0.27% increase in PSNR.

VII. CONCLUSION

In this article, the meshless collocation scheme was introduced in which DTV filter was applied in combination with Multiquadric RBF to solve nonlinear equation for the smooth solution and to remove the additive noise from the images. The proposed meshless scheme was investigated on various real and artificial images grayscale and color artificial images and the achieved results were compared with the existing traditional state-of-art schemes.

Our numerical experiments revealed that the proposed methodology produced not only good quality of image restoration but also sharply resolved the discontinuities and

improved overall accuracy. It was observed that the performance of the meshless scheme was better in image restoration quality (PSNR, SSIM, SNR, minimization of staircase effect and preservation of edges, texture, and homogeneity), iteration numbers, and computation time required for convergence compared with existing methods. The parameter sensitivity analysis was also discussed.

REFERENCES

[1] R. C. Gonzalez and R. E. Woods, *Digital Image Processing*, 3rd ed. Englewood Cliffs, NJ, USA: Prentice-Hall, 2008.

[2] X. Li, L. Li, and Q. H. Wang, "Wavelet-based iterative perfect reconstruction in computational integral imaging," *J. Opt. Soc. Amer. A, Opt. Image Sci.*, vol. 225, no. 7, pp. 1212–1220, 2018.

[3] L. M. Satapathy, P. Das, A. Shatapathy, and A. K. Patel, "Bio-medical image denoising using wavelet transform," *Int. J. Recent Technol. Eng.*, vol. 8, no. 1, pp. 2874–2879, 2019.

[4] K. Naveed, B. Shaukat, S. Ehsan, K. D. Mcdonald-Maier, and N. ur Rehman, "Multiscale image denoising using goodness-of-fit test based on EDF statistics," *PLoS ONE*, vol. 14, no. 5, May 2019, Art. no. e0216197, doi: 10.1371/journal.pone.0216197.

[5] C. Kervrann, "An adaptive window approach for image smoothing and structures preserving," in *Proc. Eur. Conf. Comput. Vis.*, 2004, pp. 132–144.

[6] J. Polzehl and K. Tabelow, "Adaptive smoothing of digital images: The R package adimpro," *J. Stat. Softw.*, vol. 19 no. 1, pp. 1–17, 2007.

[7] A. Ramadhan, F. Mahmood, and A. Elci, "Image denoising by median filter in wavelet domain," *Int. J. Multimedia Appl.*, vol. 9, no. 1, pp. 31–40, Feb. 2017.

[8] L. Luo, Z.-Q. Zhao, X.-P. Li, and X.-C. Feng, "A stochastic image denoising method based on adaptive patch-size," *Multidimensional Syst. Signal Process.*, vol. 30, no. 2, pp. 705–725, Apr. 2019.

[9] J. Bai and X.-C. Feng, "Image denoising using generalized anisotropic diffusion," *J. Math. Imag. Vis.*, vol. 60, no. 7, pp. 994–1007, Sep. 2018.

[10] F. Liu and J. Liu, "Anisotropic diffusion for image denoising based on diffusion tensors," *J. Vis. Commun. Image Represent.*, vol. 23, no. 3, pp. 516–521, Apr. 2012.

[11] L. I. S. Rudin Osher and E. Fatemi, "Nonlinear total variation based noise removal algorithms," *Phys. D, Nonlinear Phenomena*, vol. 60, nos. 1–4, pp. 159–268, 1992.

[12] G. Aubert and P. Kornprobst, *Mathematical Problems in Image Processing: Partial Differential Equations and The Calculus of Variations*. New York, NY, USA: Springer-Verlag, 2005, doi: 10.1007/978-0-387-44588-5.

[13] T. F. Chen and J. H. Shen, "Image processing and analysis," *SIAM J. Appl. Math.*, vol. 6, pp. 1–97, 2005.

[14] D. Q. Chen, L. Z. Cheng, and F. Su, "'Restoration of images based on subspace optimization accelerating augmented Lagrangian approach," *J. Comput. Appl. Math.*, vol. 235, no. 8, pp. 2766–2774, 2011.

[15] C. Wu, J. Zhang, and X. C. Tai, "Augmented Lagrangian method for total variation restoration with non-quadratic fidelity," *Inverse Problems Imag.*, vol. 5, no. 1, pp. 237–261, 2011.

[16] A. Lanza, S. Morigi, F. Sgallari, and Y. W. Wen, "Image restoration with Poisson–Gaussian mixed noise," *Comput. Methods Biomech. Biomed.*, vol. 2, no. 1, pp. 12–24, 2014.

[17] T. Wu, "Variable splitting based method for image restoration with impulse plus Gaussian noise," *Math. Problems Eng.*, vol. 2016, Nov. 2016, Art. no. 3151303, doi: 10.1155/2016/3151303.

[18] M. Zhang, Y. Liu, G. Li, B. Qin, and Q. Liu, "Iterative scheme-inspired network for impulse noise removal," *Pattern Anal. Appl.*, vol. 23, pp. 135–145, Nov. 2018.

[19] T. Chen and H. Ren Wu, "Adaptive impulse detection using center-weighted median filters," *IEEE Signal Process. Lett.*, vol. 8, no. 1, pp. 1–3, Jan. 2001.

[20] Z. Wang and D. Zhang, "'Progressive switching median filter for the removal of impulse noise from highly corrupted images," *IEEE Trans. Circuits Syst. II, Analog Digit. Signal Process.*, vol. 46, no. 1, pp. 78–80, Jan. 1999.

[21] P. Zhang and F. Li, "A new adaptive weighted mean filter for removing Salt-and-Pepper noise," *IEEE Signal Process. Lett.*, vol. 21, no. 10, pp. 1280–1283, Oct. 2014.

[22] K. K. V. Toh and N. A. M. Isa, "Noise adaptive fuzzy switching median filter for salt-and-pepper noise reduction," *IEEE Signal Process. Lett.*, vol. 17, no. 3, pp. 281–284, Mar. 2010.

[23] S. Esakkirajan, T. Veerakumar, A. N. Subramanyam, and C. H. PremChand, "Removal of high density salt and pepper noise through modified decision based unsymmetric trimmed median filter," *IEEE Signal Process. Lett.*, vol. 18, no. 5, pp. 287–290, May 2011.

[24] P. H. Lin, B. H. Chen, F. C. Cheng, and S. C. Huang, "A morphological mean in Alter for impulse noise removal," *J. Display Technol.*, vol. 12, no. 4, pp. 344–350, 2016.

[25] T. F. Chan, S. Osher, and J. Shen, "The digital TV filter and nonlinear denoising," *IEEE Trans. Image Process.*, vol. 10, no. 2, pp. 231–241, Feb. 2001.

[26] J. Sun, Q. Zhang, F. Wang, and X. Zhao, "On the generalization of digital total variation filter," in *Proc. Congr. Image Signal Process.*, May 2008, pp. 384–388, doi: 10.1109/CISP.2008.580.

[27] Q. J. Zhang Sun and G. Xu, *Advances in Geometric Modeling Processing*, vol. 6130. Berlin, Germany: Springer-Verlag, pp. 203–290, 2010, doi: 10.1007/978-3-642-13411-1.

[28] G. A. Anastassiou, I. K. Argyros, J. M. Ash, K. Bittner, and J. D. L. Cal, "Handbook of analytic computational methods in applied mathematics," in *E-publishing*. Boca Raton, FL, USA: CRC Press, 2000, pp. 751–769.

[29] S. A. Sarra, "Digital total variation filtering as postprocessing for Chebyshev pseudospectral methods for conservation laws," *Numer. Algorithms*, vol. 41, no. 11, pp. 17–33, 2005.

[30] A. Burger and T. Sonar, "Discrete filtering of numerical solutions to hyperbolic conservation laws," *Int. J. Numer. Methods Fluids*, vol. 40, nos. 1–2, pp. 263–271, 2002.

[31] S. A. Sarra, "Digital total variation filtering as postprocessing for radial basis function approximation methodss," *Comput. Math. Appl.*, vol. 52, nos. 6–7, pp. 1119–11130, 2006.

[32] A. Bürgel, T. Grahs, and T. Sonar, "From continuous recovery to discrete filtering in numerical approximations of conservation laws," *Appl. Numer. Math.*, vol. 42, nos. 1–3, pp. 47–60, 2002.

[33] E. J. Kansa, "Multiquadrics—A scattered data approximation scheme with applications to computational fluid-dynamics—I surface approximations and partial derivative estimates," *Comput. Math. with Appl.*, vol. 19, nos. 8–9, pp. 147–161, 1990.

[34] E. J. Kansa, "Multiquadrics—A scattered data approximation scheme with applications to computational fluid-dynamics—II solutions to parabolic, hyperbolic and elliptic partial differential equations," *Comput. Math. with Appl.*, vol. 19, nos. 8–9, pp. 127–145, 1990.

[35] E. J. Kansa, "Motivation for using radial basis functions to solve PDEs," Tech. Rep., 1999. [Online]. Available: http://www.rbf-pde.org/kansaweb.pdf

[36] M. A. Jankowska, A. Karageorghis, and C. S. Chen, "Kansa RBF method for nonlinear problems," *Int. J. Comput. Methods Experim. Meas.*, vol. 6, no. 6, pp. 1000–1007, Jan. 2018.

[37] M. H. Zerroukat Power and C. S. Chen, "A numerical method for heat transfer problem using collocation and radial basis functions," *Int. J. Numer. Methods. Eng.*, vol. 42, 1263-1278, 2008.

[38] E. Larsson and B. Fornberg, "A numerical study of some radial basis function based solution methods for elliptic PDEs," *Comput. Math. Appl.*, vol. 45, nos. 5–6, pp. 891–902,2003.

[39] E. Larsson and B. Fornberg, "On the efficiency and exponential convergence of multiquadric collocation method compared to finite element method," *Eng. Anal. Boundary Elements*, vol. 27, no. 3, pp. 251–257, 2003.

[40] K. Parand and J. A. Rad, "Numerical solution of nonlinear Volterra–Fredholm–Hammerstein integral equations via collocation method based on radial basis functions," *Appl. Math. Comput.*, vol.218, no. 9, pp. 5292–5309, 2012.

[41] Y. Ordokhani and M. Razzaghi, "Solution of nonlinear Volterra–Fredholm–Hammerstein integral equations via a collocation method and rationalized Haar functions," *Appl. Math. Lett.*, vol. 21, no. 1, pp. 4–9, 2008.

[42] E. Houstis, "A collocation method for systems of nonlinear ordinary differential equations," *J. Math. Anal. Appl.*, vol. 62, no. 1, pp. 24–37, 1978.

[43] M. R. Eslahchi, M. Dehghan, and M. Parvizi, "Application of the collocation method for solving nonlinear fractional integro-differential equations," *J. Comput. Appl. Math.*, vol. 257, pp. 105–128, Feb. 2014.

[44] E. H. Doha, D. Baleanu, A. H. Bhrawy, and M. A. Abdelkawy, "A jacobi collocation method for solving nonlinear burgers-type equations," *Abstract Appl. Anal.*, vol. 2013, pp. 1–12, 2013.

[45] M. D. Buhmann, *Radial Basis Functions: Theory and Implementations*, vol. 2. Cambridge, U.K.: Cambridge Univ. Press, 2003.
[46] W. Z. J. Chen Fu and C. S. Chen, *Recent Advances in Radial Basis Function Collocation*. Berlin, Germany: Springer-Verlag, 2013, doi: 10.1007/978-3-642-39572-7.
[47] C. Michelle, "Interpolation of scattered data: Distance matrices and conditionally positive definite functions," *Construct. Approximation*, vol. 2, pp. 11–12, 1986.
[48] W. R. Madych and S. A. Nelson, "Multivariate interpolation and conditionally positive definite functions. II," *Math. Comput.*, vol. 54, no. 189, pp. 211–230, 1990.
[49] S. Rippa, "An algorithm for selecting a good value for the parameter c in radial basis function interpolation," *Adv. Comput. Math.*, vol. 11, nos. 2–3, pp. 193–210, Nov. 1999.
[50] M. Uddin, "On the selection of a good value of shape parameter in solving time-dependent partial differential equations using RBF approximation method," *Appl. Math. Model.*, vol. 38, no. 1, pp. 135–144, 2014.
[51] R. Dosselmann and X. D. Yang, "A comprehensive assessment of the structural similarity index," *Signal, Image Video Process.*, vol. 5, no. 1, pp. 81–91, Mar. 2011.
[52] Z. Wang, A. C. Bovik, H. R. Sheikh, and E. P. Simoncelli, "Image quality assessment: From error visibility to structural similarity," *IEEE Trans. Image Process.*, vol. 13, no. 4, pp. 600–612, Apr. 2004.
[53] S. Osher and S. Shen, "Digitized PED method for data restoration," in *E-publishing*, G. Anastassiou, Ed. Boca Raton, FL, USA: CRC Press, 2000, pp. 751–769.
[54] G. Yuan and B. Ghanem, "A new method for image restoration in the presence of impulse noise," in *Proc. IEEE Conf. Comput. Vis. Pattern Recognit.*, vol. 1, Jun. 2015, pp. 5369–5377.
[55] J.-L. Yin, B.-H. Chen, and Y. Li, "Highly accurate image reconstruction for multimodal noise suppression using semisupervised learning on big data," *IEEE Trans. Multimedia*, vol. 20, no. 11, pp. 3045–3056, Nov. 2018.
[56] C. L. P. Chen, L. Liu, L. Chen, Y. Yan Tang, and Y. Zhou, "Weighted couple sparse representation with classified regularization for impulse noise removal," *IEEE Trans. Image Process.*, vol. 24, no. 11, pp. 4014–4026, Nov. 2015.

MUSHTAQ AHMAD KHAN received the Ph.D. degree from the School of Engineering Mechanics and Materials, Hohai University, China. He is currently teaching at the Department of Electrical Engineering, University of Engineering and Technology, Mardan, Pakistan. His research interest includes modeling and numerical simulation, and the use of mesh-based and meshless schemes in variational and filter-based image restoration.

AHMED B. ALTAMIMI received the Ph.D. degree in electrical and computer engineering from the University of Victoria, Victoria, BC, Canada, in 2014. He is currently holding an Associate Professor Position with the College of Computer Science and Engineering, University of Hail, Hail, Saudi Arabia. His research interests include routing and mobility modeling in wireless networks, and security and privacy threats in Internet of things (IoT) environment and intelligent transportation systems.

ZAWAR HUSSAIN KHAN received the Ph.D. degree in electrical engineering from the University of Victoria, Victoria, BC, Canada, in 2016. He is currently working as an Assistant Professor with the Department of Electrical Engineering, University of Engineering and Technology Peshawar. His research interests include intelligent transportation and communication systems.

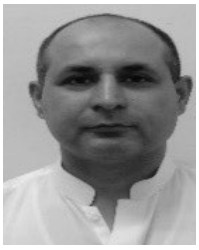

KHURRAM SHEHZAD KHATTAK received the Ph.D. degree from The George Washington University, DC, USA, in 2017. He is currently working as an Assistant Professor with the Department of Computer Systems Engineering, University of Engineering and Technology Peshawar. His research interests include intelligent transportation systems, the Internet of Things (IoT), and embedded systems.

MURTAZA ALI received the Ph.D. degree in graph theory from the National University of Computer and Emerging Sciences, Peshawar, Pakistan. He is currently an Assistant Professor with the University of Engineering and Technology, Mardan, Pakistan. His research interests are in applied graph theory, combinatorics, algorithm analytical-order PDEs, and fast numerical methods for the solution of integral order and fractional order PDEs.

ASMAT ULLAH received the Ph.D. degree in engineering mechanics from Hohai University, Nanjing, China. He is currently working as a Subject Specialist/Lecturer in mathematics with Education Department. His research interests include image de-noising, image segmentation, image dehazing, fractional-order PDEs, and fast numerical methods for the solution of integral order and fractional order PDEs.

SHERAZ KHAN is currently pursuing the Ph.D. degree in telecommunication engineering with the Asian Institute of Technology (AIT), Thailand. He is currently an Assistant Professor with the University of Engineering Technology (UET), Mardan, Pakistan. His research interests include wireless regional area networks (WRANs), communications TV white spaces (TVWS) and smart grid communications, and theoretical computer science.

MUHAMMAD SOHAIL KHAN received the Ph.D. degree from Jeju National University, South Korea. He is currently an Assistant Professor with the Department of Computer Software Engineering, University of Engineering and Technology, Mardan, Pakistan. The major focus of his work is the investigation and application of alternate programming strategies to enable the involvement of masses in the Internet of Things application design and development. End-user programming, human–computer interactions, and empirical software engineering are also included in his research interests.

MUHAMMAD FAISAL ABRAR is currently pursuing the Ph.D. degree with the Department of Computer Software Engineering, University of Engineering and Technology Peshawar (Mardan Campus), under the supervision of Asst. Prof. Muhammad Sohail Khan. He was a Lecturer with the University of Swat and the University of Buner. He is currently a Lecturer with the University of Engineering and Technology Mardan, Pakistan. His research interests include agile software development, software quality assurance, software outsourcing partnership, empirical software engineering, systematic literature review, big data, and machine learning.